P-type Calcium Channels in the Somata and Dendrites of Adult Cerebellar Purkinje Cells

Maria M. Usowicz, Mutsuyuki Sugimori,
Bruce Cherksey, and Rodolfo Llinás
Department of Physiology and Biophysics
New York University Medical Center
New York, New York 10016

Summary

The pharmacological and single-channel properties of Ca^{2+} channels were studied in the somata and dendrites of adult cerebellar Purkinje cells. The Ca^{2+} channels were exclusively of the high threshold type: low threshold Ca^{2+} channels were not found. These high threshold channels were not blocked by ω-conotoxin GVIA and were inhibited rather than activated by BAY K 8644. They were therefore pharmacologically distinct from high threshold N- and L-type channels. Funnel web spider toxin was an effective blocker. The channels opened to conductance levels of 9, 14, and 19 pS (in 110 mM Ba^{2+}). These slope conductances were in the range of those reported for N- and L-type channels. Our results are in agreement with previous reports suggesting that Ca^{2+} channels in Purkinje cells can be classified as P-type channels according to their pharmacology. The results also suggest that distinctions among Ca^{2+} channel types based on the single-channel conductance are not definitive.

Introduction

Voltage-activated Ca^{2+} channels in mammalian neurons govern many physiological processes, such as transmitter release and neuronal integration (Llinás, 1988; Tsien and Tsien, 1990; Bertolino and Llinás, 1992). The multiple types of neuronal Ca^{2+} channels that have been demonstrated according to their functional properties are the low threshold T type and the high threshold N, L, and P type (Llinás and Yarom, 1981; Carbone and Lux, 1984a, 1984b; Fedulova et al., 1985; Nowycky et al., 1985a; Fox et al., 1987a, 1987b; Llinás et al., 1989). The distinctive properties of T-, N-, and L-type channels have been derived from many whole-cell and single-channel patch-clamp studies (Bean, 1989; Hess, 1990; Carbone et al., 1990; Usowicz et al., 1990; Regan et al., 1991; Bertolino and Llinás, 1992; Kasai and Neher, 1992). P-type channels were defined as the channels underlying the high threshold Ca^{2+} action and plateau potentials in adult cerebellar Purkinje cells (Llinás et al., 1989, 1992). These potentials were shown to be insensitive to blockers of N- or L-type channels, but could be inhibited by purified funnel web spider toxin (FTX). Comparatively little is known about the functional properties of P-type channels, since there have been few studies of whole-cell P-type channel currents (Regan, 1989, 1991; Mintz et

al., 1992a, 1992b) and no unitary recordings of P-type channels in Purkinje cells.

Ca^{2+} channels expressed in Xenopus laevis oocytes from rat brain mRNA, the cloned BI brain Ca^{2+} channel expressed in Xenopus oocytes, P-type channels incorporated into lipid bilayers, and P-type channels in Purkinje cells have similar pharmacological profiles (Llinás et al., 1989; Lin et al., 1990; Mori et al., 1991; Mintz et al., 1992a, 1992b). However, a comparison of the biophysical characteristics of these channels is not straightforward, since the Ca^{2+} channel currents have been recorded in different preparations (Purkinje cells, oocytes, and bilayers) with different Ba^{2+} concentrations (see Tsien et al., 1991).

There is presently no consensus regarding the types of voltage-activated Ca^{2+} channels present in cerebellar Purkinje cells. Different conclusions have been reached on the basis of experiments in adult cells (Llinás and Sugimori, 1980a, 1980b; Llinás et al., 1989), in freshly dissociated somata of young Purkinje cells (Regan, 1989, 1991; Kaneda et al., 1990; Mintz et al., 1992a, 1992b), and in cultured Purkinje cells derived from embryonic or newborn animals (Bossu et al., 1989a, 1989b; Hirano and Hagiwara, 1989; Hockberger et al., 1989). These differences probably occur because Purkinje cells express different channels under the various conditions.

To characterize P-type channels and to address these issues, we have made patch-clamp recordings from adult cerebellar Purkinje cells. The aim was to describe Ca^{2+} channels not only in the soma, but also in the dendrite, since the electrical activity of Purkinje cells under physiological conditions is dominated by dendritic Ca^{2+} channels (Llinás and Sugimori, 1980a, 1980b; Ross and Werman, 1987; Tank et al., 1988; Hockberger et al., 1989; Sugimori and Llinás, 1990). We report biophysical, pharmacological, and single-channel properties and compare them with the properties of previously defined Ca^{2+} channels.

Results

Identification and Preparation of Cells

Voltage-activated Ca^{2+} channel currents were recorded in cell-attached patches (Hamill et al., 1981) from young adult, fully differentiated Purkinje cells in thin sagittal cerebellar slices of the guinea pig. The neurons were readily identified according to their morphology and position in the slice. Recordings were made from one of two sites on a neuron: the soma or the dendrite at a bifurcation. These were cleaned as described by Edwards et al. (1989). Figure 1 is a photograph of a Purkinje cell, after the soma and part of the dendritic tree were cleaned. Removal of the overlying tissue enabled a clear view of the soma, from which emerged a single dendrite that bifurcated
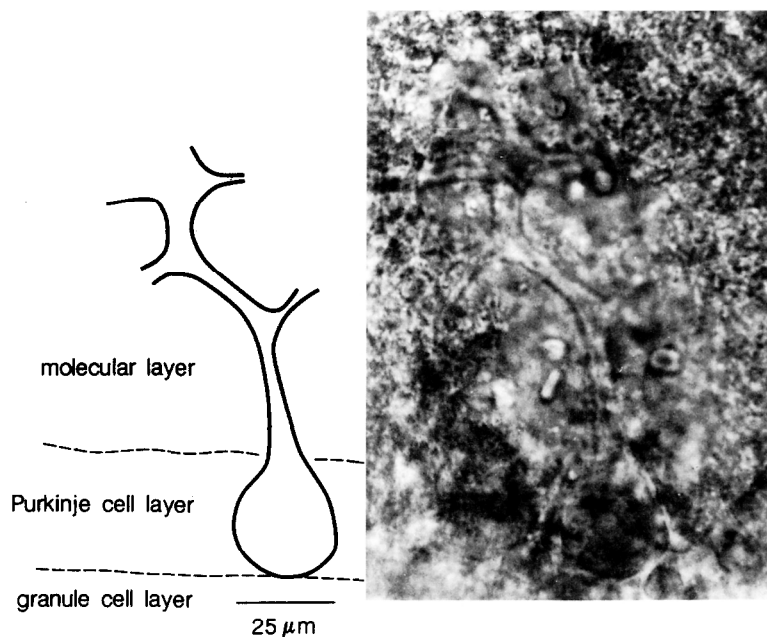
Figure 1. Appearance of an Exposed Adult Purkinje Cell in a Parasagittal Cerebellar Slice (~ 150 μm Thick) from a Guinea Pig

The soma and primary, secondary, and tertiary bifurcations of the dendrite were exposed by alternately puffing and sucking bath solution from a pipette to loosen and remove overlying tissue. Bar, 25 μm.

molecular layer

Purkinje cell layer

granule cell layer

25 μm

after traversing the molecular layer for 30 μm and again after a further 20 μm. All dendritic recordings described were from such bifurcations, for a number of reasons. First, the dendrite was widest at these dividing points (Figure 1). It was therefore less difficult to aim the pipette at these areas than at the other thinner parts of the dendrite. Second, bifurcations were easily recognized, so that pipettes were localized to specific parts of the dendrite. Third, the distance from the recording site to the soma was easier to gauge. However, the acquisition of good quality dendritic recordings was a laborious process given the small diameter of the bifurcation sites that we recorded from (6–8 μm) compared with that of the somata (20–30 μm) (see Figure 1).

Inactivation

To examine time-dependent inactivation of the Ca^{2+} channels, currents were evoked in multichannel patches with relatively long depolarizing voltage jumps, 600–1100 ms in duration, applied from a membrane potential held 30 mV negative to the resting potential of the cell. The currents (carried by 110 mM Ba^{2+}, n = 3 somata) occurred throughout the duration of the jump, as exemplified by the individual current traces in Figure 2A. The lack of inactivation is seen better in Figure 2B, which shows average current records at different test potentials (same patch as in Figure 2A). Stronger depolarization had little effect on current decay: at potentials up to +40 mV, the average records are flat; at +40 mV, the current decays by ~15% during 1100 ms.

Voltage-ramp experiments also indicated little inactivation of Ca^{2+} channels in Purkinje cells. That is, Ca^{2+} channel currents elicited in multichannel patches with depolarizing voltage ramps were similar in size to curre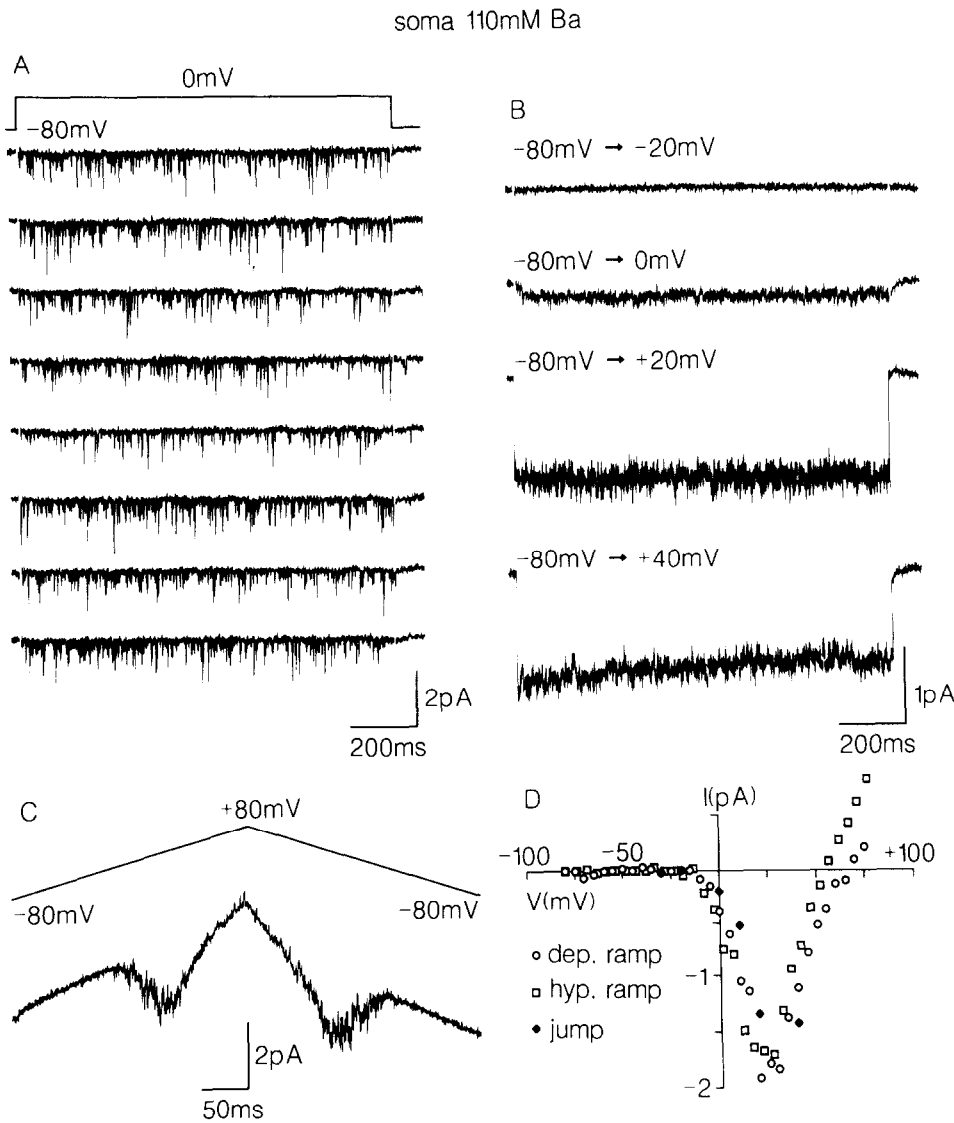nts produced by hyperpolarizing voltage ramps (110 mM Ba^{2+}, n = 6 somata, n = 2 dendrites; 10 mM Ba^{2+}, n = 5 somata, n = 1 dendrite), as exemplified by the mean current trace in Figure 2C. (If the depolarizing ramp had caused inactivation, the current during the hyperpolarizing ramp would have been smaller than that during the depolarizing ramp.) Figure 2D compares the Ca^{2+} channel current generated by the depolarizing ramp with the current during the hyperpolarizing ramp, after subtraction of a linear leak current. There is good agreement at potentials up to ~+40 mV. The difference at potentials more positive than +40 mV and the vertical shift in Figure 2C of the current during the hyperpolarizing ramp relative to that during the depolarizing ramp are due to the ramp-induced capacitance currents, which were only partially compensated during recording (to be described elsewhere).

The lack of inactivation indicated that macroscopic current–voltage (I–V) relationships could be obtained from voltage-ramp experiments. The accuracy of the I–V curve determined in this way is illustrated in the plot in Figure 2D. It shows close correspondence between the currents during the ramps in Figure 2C (after linear leak current subtraction) and the amplitudes of the mean currents in Figure 2B.

I–V Relationship

Depolarizing and hyperpolarizing ramps were applied at a rate of 0.63 mV/ms to all patches described in this paper to test for current symmetry (Figure 2C). During these ramps, the threshold of activation and the potential at the peak of the I–V curve agreed to within 5 mV. Therefore, only the depolarizing ramps are described after Figure 2.

Figure 3 shows examples of multichannel currents

soma 110mM Ba

A
0mV
-80mV

B
-80mV → -20mV

-80mV → 0mV

-80mV → +20mV

-80mV → +40mV

2pA
200ms

1pA
200ms

C
+80mV
-80mV   -80mV

2pA
50ms

D
I(pA)
-100   -50   +100
V(mV)

o dep. ramp
□ hyp. ramp
• jump

-1

-2

Figure 2. Ca²⁺ Channels in Adult Cerebellar Purkinje Cells Do Not Inactivate during 1 s

(A) Single-channel currents carried by 110 mM Ba²⁺ in a multichannel somatic patch, elicited with consecutive depolarizing voltage jumps to 0 mV, 1100 ms in duration, applied once every 5 s. The holding potential was set 30 mV negative to the resting potential.
(B) Mean current records at different test potentials, obtained by averaging between 24 and 28 traces. Same patch as in (A).
(C) Mean record of 8 traces recorded with 110 mM Ba²⁺ during depolarizing and hyperpolarizing voltage jumps applied to a multichannel somatic patch once every 5 s.
(D) Ca²⁺ channel currents recorded during the depolarizing ramp (open circles) and the hyperpolarizing ramp (open squares) in (C), after correction for linear leak current. For clarity, current is plotted every ~5 mV. The amplitudes of mean currents evoked by voltage jumps shown in (B) are indicated by closed diamonds. The current at +40 mV was measured at its peak.
R_p, 4 MΩ (A and B); 7 MΩ (C). R_s, 200 GΩ (A and B). Filter, 500 Hz (A and B); 1.9 kHz (C).

carried by 110 mM Ba²⁺ during voltage ramps applied to a patch at a dendritic bifurcation (Figure 3A) and to a somatic patch (Figure 3B). The currents show a single peak that occurred, on average, at +5 mV (n = 2) in the dendrite and at +10 ± 3 mV (n = 5, ± SEM) in the soma. The currents started to activate, on average, at -21 mV (n = 2) in the dendrite and at -15 ± 2 mV (n = 6) in the soma. It is difficult to compare these currents with macroscopic whole-cell Ca²⁺ channel currents that are usually recorded with lower concentrations of Ba²⁺ or Ca²⁺. Therefore, some somatic recordings

were made with 10 mM Ba²⁺ as the charge carrier. Examples are shown in Figure 3C. On average, these currents in 5 somatic patches activated at -41 ± 3 mV and showed a single peak at -4 ± 2 mV. The shift of the I-V curve toward negative potentials presumably reflects, in part, the less effective screening of the negative membrane surface charge by 10 mM Ba²⁺ than by 110 mM Ba²⁺.

Single-Channel Conductance
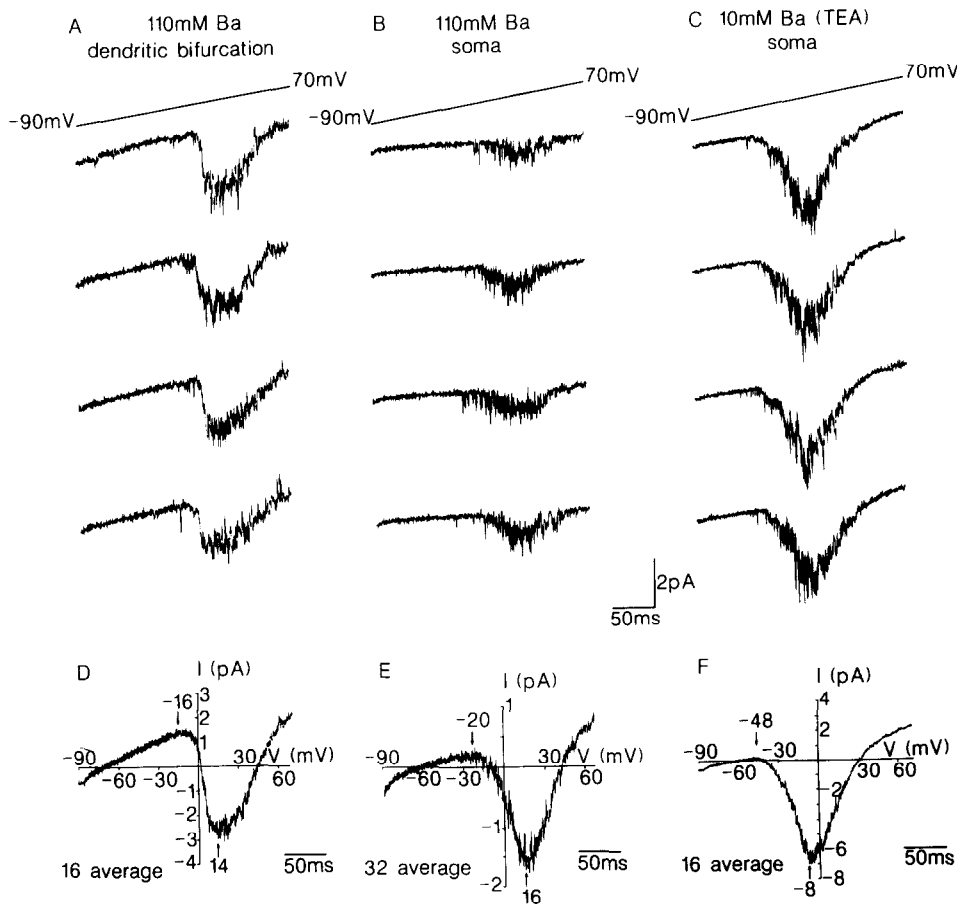To examine currents through individual Ca²⁺ chan-

A   110mM Ba
        dendritic bifurcation

B   110mM Ba
              soma

C   10mM Ba (TEA)
              soma

_70mV   _70mV   _70mV

-90mV   -90mV   -90mV

2pA

50ms

D   I (pA)   E   I (pA)   F   I (pA)

-16 3   -20   -48 4
      2   1   2
-90   30 V (mV)   -90   30 V (mV)   -90   -30   V (mV)
  -60 -30   60   -60 -30   60   -60   30 60
      -2   -1   -2
      -3   -4
16 average -4 14   50ms   32 average -1   50ms   16 average   -6   50ms
                                        -2   -8 -8
                                          16

Figure 3. I–V Relationship for Ca^{2+} Channel Currents in the Dendrites and Somata of Adult Cerebellar Purkinje Cells

Cell-attached recordings in membrane patches with several Ca^{2+} channels. The membrane potential was held 30 mV negative to the resting potential, and depolarizing voltage ramps (160 mV over ~250 ms) were applied once every 5 s. (A and B) Currents recorded with 110 mM Ba^{2+} from a patch at a dendritic bifurcation and from a somatic patch. (C) Currents recorded in a somatic patch with a 10 mM Ba^{2+} pipette solution in which the other cation was TEA. (D, E, and F) Ensemble averages of currents elicited in the patches depicted above in (A), (B), and (C). Arrows indicate potentials at which the currents activate and are maximal. R_p, 6–10 MΩ. Filter, 1.9 kHz.

nels, recordings were made with higher resistance electrodes in an attempt to reduce the area of the patch and hence the number of channels in it. The currents thus recorded during depolarizing voltage jumps showed openings to more than one amplitude level. Three could be resolved, irrespective of whether the currents were evoked from a holding potential of −90 mV or −60 mV. The traces in Figure 4 are selected currents (110 mM Ba^{2+}) from a somatic patch (Figure 4A) and from a patch at a dendritic bifurcation (Figure 4B). The openings occurred throughout the duration of the ~70 ms jump. Three current levels are indicated by the solid, dashed, and dotted lines. Single-channel current amplitudes measured in 8 somatic patches and 5 dendritic patches have been plotted against patch potential in Figure 4. The slope conductances calculated from these pooled data are 9, 13, and 19 pS for channels in the soma and 10, 14, and 18 pS for channels in the dendrite.

It was difficult to obtain patches containing only a single channel. Many recordings showed superim-

posed openings, indicative of multiple channels. This is consistent with tight clustering of the Ca^{2+} channels. Furthermore, it is probable that given the relative brevity of the openings, any direct transitions between the levels were undetected. There is, therefore, no clear evidence that the different conductances are sublevels of a single type of channel. Neither is there any unequivocal evidence against this notion. However, the simplest interpretation for now may be that each conductance represents a different type of channel.

Single Ca^{2+} channel currents were usually evoked by voltage jumps to −30 mV or above. This is slightly more negative than the activation threshold of ~−15 mV for 110 mM Ba^{2+} currents during voltage ramps. The modest discrepancy occurs because the average of the infrequent brief openings at −30 to −20 mV is too small to be seen in the averaged multichannel currents evoked by voltage ramps. For instance, the traces in Figure 2A suggest a high level of channel activity at 0 mV. However, the mean current of 28 of
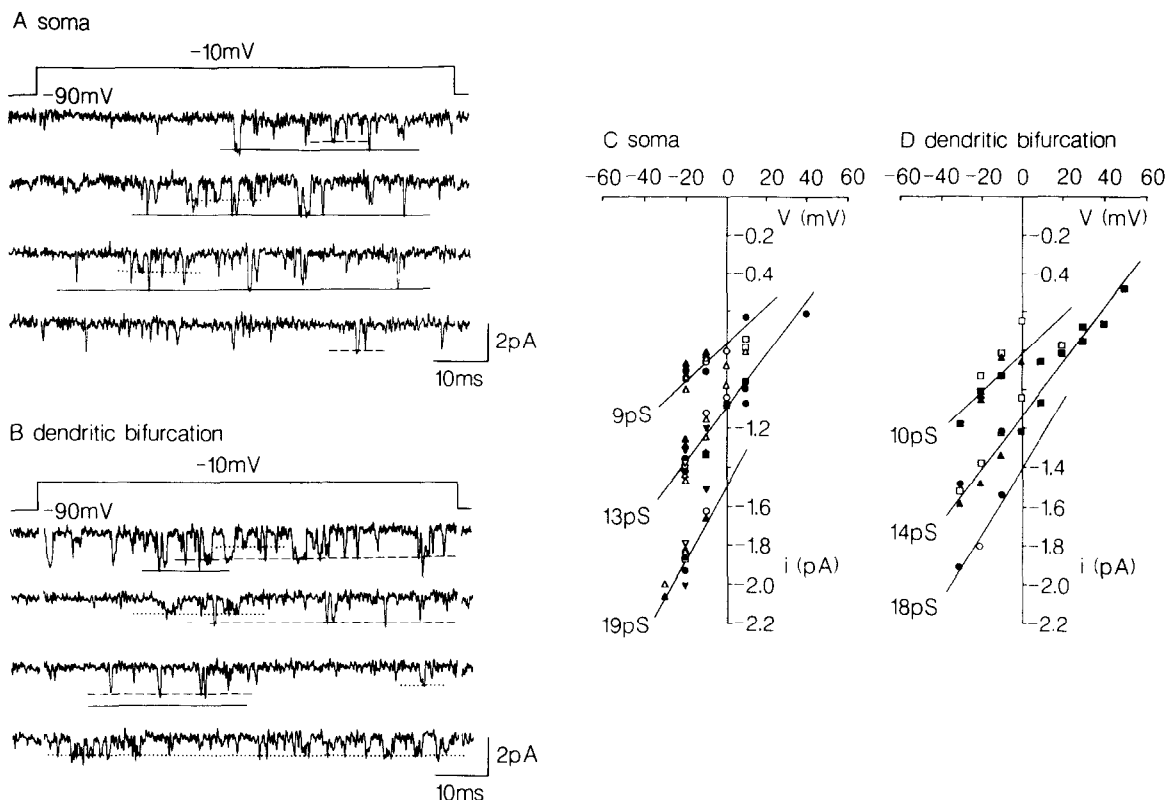
Figure 4. Multiple Conductance Openings of Ca²⁺ Channels in the Somata and Dendrites of Adult Cerebellar Purkinje Cells

(A) Single Ca²⁺ channel currents carried by 110 mM Ba²⁺ in a somatic patch, evoked by voltage jumps (~70 ms) applied once every 5 s. Three open levels are indicated by solid, dashed, and dotted lines. A level cannot be assigned to all openings. For example, the currents in the third trace in (B) may be brief openings to the "dashed level" or partially resolved openings to the "solid line."

(B) Currents in a dendritic patch. Same conditions as in (A). R_p, 12 MΩ (A); 9 MΩ (B). R_s, 130 GΩ (A); 65 GΩ (B). Filter, 2 kHz. partially resolved openings to the "solid line." R_p, 12 MΩ (A); 9 MΩ (B). R_s, 130 GΩ (A); 65 GΩ (B). Filter, 2 kHz.

(C and D) Voltage dependence of the current levels illustrated in (A) and (B). Pooled data from 8 somatic and 5 dendritic patches. Different symbols are measurements from different patches, at holding potentials set 30 mV negative to the resting potential or set at the resting potential. The indicated conductances are the slopes of the lines through the points. The 13–14 pS points were fitted with a least-squares line. The lines through the 9–10 pS and 18–19 pS data were drawn so that their extrapolated reversal potentials were the same as that of the 13–14 pS level. The resultant slopes differed from their least-squares values by less than 1 pS (the 10, 18, and 19 pS levels) or by 3 pS (the 9 pS level).

these traces, shown in Figure 2B, is relatively small and is only 0.10 of the peak of the I–V in Figure 2D.

Pharmacology of Ca²⁺ Channels

The presence of T-type Ca²⁺ channels in adult Purkinje cells can be excluded on the basis of the biophysical properties described so far. Ca²⁺ channels in Purkinje cells show little time-dependent inactivation, unlike T-type channels. The threshold of activation is more positive, by about 30 mV, than that of T-type channels in both 110 mM Ba²⁺ and 10 mM Ba²⁺ (Fox et al., 1987a, 1897b). Indeed, the properties of Ca²⁺-mediated action and plateau potentials in adult Purkinje cells are different from those of low threshold spikes (Llinás and Yarom, 1981). The unitary conductances and the threshold of activation are, however, similar to those of high threshold N-type Ca²⁺ channels (Fox et al., 1987a, 1987b). Furthermore, while the threshold of activation of the channels in 110 mM Ba²⁺ is more negative, by 20 to 30 mV, than that of high threshold L-type

Ca²⁺ channels in the absence of dihydropyridine (DHP) agonists (Fox et al., 1987a, 1987b; Plummer et al., 1989), the 18–19 pS conductance level is in the range of unitary conductances reported for L-type channels (Bean, 1989). Therefore, to characterize the high threshold Ca²⁺ channels in Purkinje cells, it was necessary to examine the sensitivity of these channels to drugs selective for N-type and L-type Ca²⁺ channels.

For the pharmacological experiments, drugs were included in the cell-attached recording pipette, or they were superfused over the cell after cleaning, before cell-attached recording, at concentrations known to be maximally effective on N-type or L-type channels. Control currents in drug-free patches were always recorded from the same set of slices and with the same set of pipettes used in the pharmacological experiments.

ω-Conotoxin GVIA

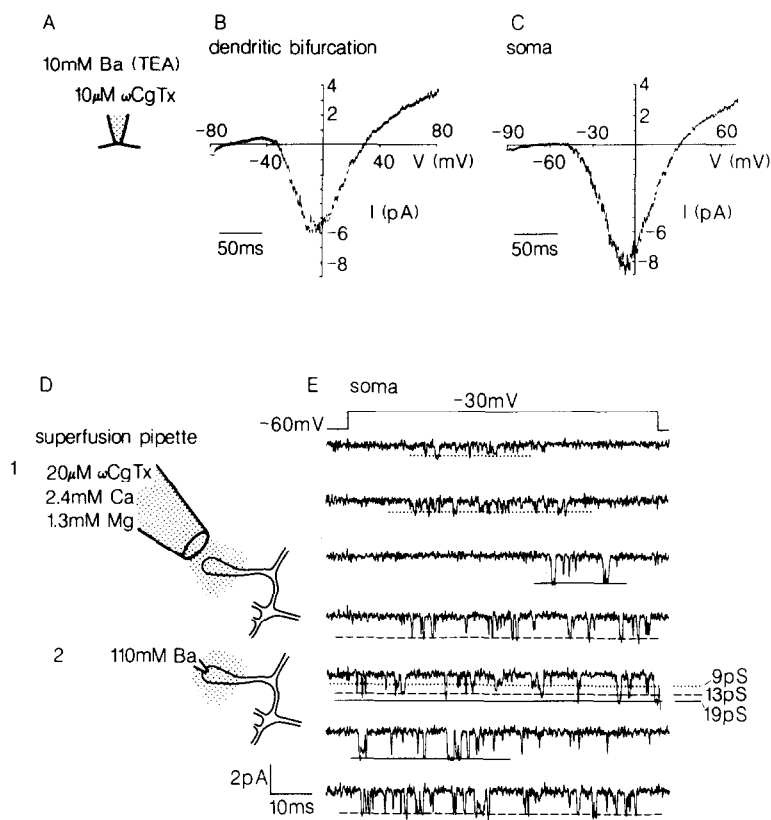ω-Conotoxin GVIA (ω-CgTx) blocks N-type channels

Figure 5. Ca^{2+} Channel Currents in the Dendrites and Somata of Adult Purkinje Cells Are Not Blocked by ω-CgTx

(A) 10 μM ω-CgTx was added to the 10 mM Ba^{2+} pipette solution, in which the other cation was TEA.

(B and C) Averages of 9 current traces in a dendritic patch and 17 in a somatic patch. Currents were evoked in multichannel patches by depolarizing voltage ramps once every 5 s. R_p, 12 MΩ (B and C). R_s, 160 GΩ (B); 110 GΩ (C). Filter, 0.7 kHz (B); 1.9 kHz (C).

(D) 1: 20 μM ω-CgTx was dissolved in the bathing medium (containing the indicated concentrations of divalent cations) and was perfused over the soma from a large pipette for 3–5 min. 2: Cell-attached recordings were then made with a 110 mM Ba^{2+} pipette solution. During this protocol, bath perfusion was stopped.

(E) Single-channel currents recorded in the manner described in (D). Three conductance levels are indicated by the solid, dashed, and dotted lines.
R_p, 8 MΩ. R_s, 170 GΩ. Filter, 2 kHz.

but not L-type channels (Aosaki and Kasai, 1989; Plummer et al., 1989; Regan et al., 1991). High concentrations of divalent cations reduce the binding of ω-CgTx to N-type channels (Abe et al., 1986; Knaus et al., 1987; Wagner et al., 1988; McCleskey et al., 1987; Marqueze et al., 1988). Therefore, two approaches were taken to avoid a false-negative result when examining the sensitivity of Ca^{2+} channels in Purkinje cells to ω-CgTx.

In the first, the concentration of Ba^{2+} in the pipette was kept relatively low at 10 mM Ba^{2+} (Figure 5A). ω-CgTx (10 μM) included in this pipette solution did not abolish the Ba^{2+} currents, as illustrated by the averaged multichannel currents evoked by voltage ramps in a dendrite (Figure 5B) and in a soma (Figure 5C). With 10 μM ω-CgTx, the peak current in the dendritic patch was −6.7 pA, while the averaged peak current in 3 somatic patches was −9.4 ± 0.3 pA. In comparison, the average control current in 5 somatic patches was −4.6 ± 1.4 pA. The I-V curve was unchanged by ω-CgTx. The dendritic current activated at −44 mV and was maximal at −9 mV, while somatic currents activated at −43 ± 5 mV and peaked at −2 ± 6 mV. The values are comparable to those measured in the absence of ω-CgTx (given above). These results indicated that Ca^{2+} channels in Purkinje cells were, for the most part, not ω-CgTx-sensitive N-type channels.

In a second approach (Figure 5D), 20 μM ω-CgTx was superfused over the cell for 3 min or longer from a large pipette positioned ~20 μm away from the membrane (3 μM was used in 3 out of 10 experiments).

ω-CgTx was dissolved in the bathing medium, which contained relatively low concentrations of divalent cations. As soon as possible after stopping the perfusion with ω-CgTx, usually within 30 s, cell-attached recordings were made with a 110 mM Ba^{2+} pipette solution. Bath perfusion was discontinued during this procedure to minimize diffusion of ω-CgTx away from the neuron. This paradigm is known to be effective in inhibiting N-type channels in dorsal root ganglion neurons (McCleskey et al., 1987; Aosaki and Kasai, 1989), as binding of ω-CgTx is essentially irreversible (Knaus et al., 1987; Wagner et al., 1988). Figure 5E shows examples of single-channel currents in a somatic patch exposed to ω-CgTx in the way just described. Multiple conductance openings are visible, indicating that all of the three conductance levels were insensitive to inhibition by ω-CgTx. This result is typical of a total of 9 somatic patches and 1 dendritic patch.

Dihydropyridines

The 1,4-DHP compounds are selective agonists or antagonists of L-type Ca^{2+} channels (Bechem et al., 1988; Triggle and Ramp, 1989; Porzig, 1990). Ca^{2+} channel currents were recorded with the agonist BAY K 8644 (1–3 μM, n = 8 somata, n = 2 dendrites) in the 110 mM Ba^{2+} pipette solution. Figure 6 shows examples of currents recorded in the presence of 1 μM BAY K 8644 from a somatic patch (Figure 6A) and from a dendritic patch (Figure 6C). They are not obviously different
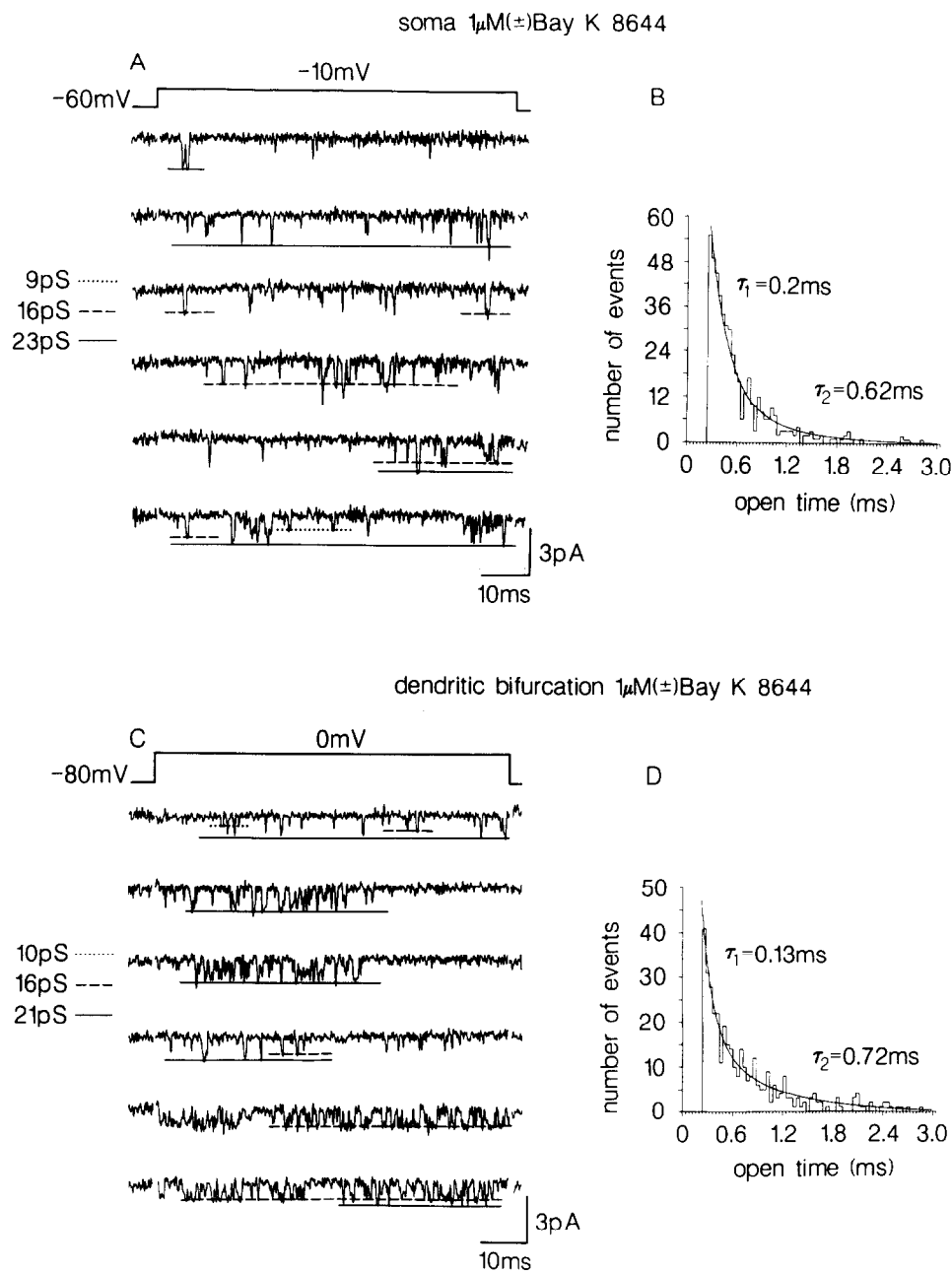
Figure 6. Openings of Single Ca²⁺ Channels in Purkinje Cells Are Not Prolonged by BAY K 8644

(A) Single channel currents recorded in a somatic patch with a 110 mM Ba²⁺ pipette solution containing 1 μM (±) BAY K 8644. Openings are to three conductance levels of 9, 16, and 23 pS, calculated as slope conductances from the I–V plots for this patch.
(B) Open time distribution obtained for currents in the patch depicted in (A) at −10 mV, fitted with two exponential components.
(C and D) Data from a patch at a dendritic bifurcation. Same conditions as in (A) and (B). R_p, 10–13 MΩ. R_s, 120 GΩ (A); 150 GΩ (B). Filter, 1.9 kHz (A and C); 2.3 kHz (B and D).

from currents in the absence of BAY K 8644 shown in the earlier figures. Most are briefer than 5 ms (compare with the calibration bar) and are therefore much briefer than the 10–100 ms openings of L-type channels usually induced by BAY K 8644 (Brown et al., 1984; Hess et al., 1984; Nowycky et al., 1985b). Figures 6B and 6D show open time distributions for the data shown in Figures 6A and 6C. Durations of openings to all conductance levels were included. The histograms

were fitted with the sum of two exponentials with time constants of $\tau_1 = 0.2$ ms and $\tau_2 = 0.62$ ms for channels in the soma and $\tau_1 = 0.13$ ms and $\tau_2 = 0.72$ ms for channels in the dendrite ($V_m = -10$ or 0 mV). It is certain that these values are not reliable estimates of the true mean open time, given that many short openings (and closings) have been excluded from the histogram. Nevertheless, these time constants are much shorter than those reported for L-type channels

in the presence of BAY K 8644, which, for example, are characterized by a mean open time of 20–60 ms (maximum voltage = −10 to +10 mV; Hess et al., 1984; Nowycky et al., 1985b).

It was surprisingly difficult to record Ca^{2+} channel activity in the presence of BAY K 8644. When it was included in the pipette solution, only 2 out of 11 somatic patches showed clear currents when depolarized from a holding potential set at the resting potential of the cell. Currents were seen briefly, for less than 90 s after sealing the pipette onto the cell, in 5 patches, but were absent from another 4. Likewise, in the dendrite, currents were observed transiently in 1 patch but not in 3 patches. Without BAY K 8644 in the pipette, unitary Ca^{2+} channel currents were observed in the same sets of slices from the same holding potential (set at the resting potential of the cell) in 4/5 somatic patches and in 2/3 dendritic patches. In other experiments, BAY K 8644 was included in the bathing medium. In this situation, with the holding potential set at the resting potential of the cell, Ba^{2+} currents were absent in 5 somatic patches, or they were present transiently for 1 or 2 voltage jumps or intermittently in 4 somatic patches. In other slices of the same set that were not exposed to BAY K 8644, currents were present in 4/4 somatic patches.

The experiments with BAY K 8644 indicate that Ca^{2+} channels encountered in this preparation were not of the L type. Although the BAY K 8644 that we used was a racemate of an agonist S-(−)-enantiomer and an antagonist R-(+)-enantiomer, the potentiation of any L-type channels present would have been visible, since the effects of the agonist enantiomer are usually predominant (Bechem et al., 1988). Our experiments also suggest that BAY K 8644 is an antagonist of Purkinje cell Ca^{2+} channels. This is not without precedent: Bay K 8644 inhibits high threshold currents (Boll and Lux, 1985), N-type channels (Aosaki and Kasai, 1989; Jones and Jacobs, 1990), and the cloned BI brain Ca^{2+} channel (Mori et al., 1991). From our preliminary data, it is unclear whether the inhibition was due to nonselective effects at the relatively high concentrations used or to a shift of the steady-state inactivation curve (Bechem et al., 1988).

Funnel Web Spider Toxin

The experiments with ω-CgTx and BAY K 8644 indicated that Ca^{2+} channels in adult Purkinje cells are pharmacologically distinct from N-type and L-type channels. Next, we tested the effect of purified FTX, which can inhibit Ca^{2+}-dependent action and plateau potentials in Purkinje cells (Llinás et al., 1989). FTX, a polyamine, was purified from crude venom of American funnel web spiders, Agelenopsis aperta, as described previously (Llinás et al., 1989; Cherksey et al., 1991). The eluted fractions were screened for inhibitory activity against Ca^{2+} spikes in Purkinje cells, recorded with intracellular microelectrodes, and the most effective was used in the patch-clamp experiments. To enhance the effectiveness of FTX, the con-

centration of Ba^{2+} in the pipette solution (Figure 7) was reduced from 110 mM (Lin et al., 1990) and the other cation in the pipette solution was Na^+ rather than tetraethylammonium (TEA) (Cherksey, Sugimori, and Llinás, unpublished data). We chose to record with 20 mM rather than with 10 mM Ba^{2+} (as in experiments with ω-CgTx), because outward K^+ currents were reduced more effectively, albeit incompletely, by 20 mM Ba^{2+} than by 10 mM Ba^{2+}.

Figure 7A shows superimposed currents evoked by depolarizing voltage ramps in 2 somatic patches with different concentrations of FTX in the pipette. The inward current in the presence of a 1:500 dilution (see Experimental Procedures) of purified FTX was markedly smaller than the current recorded with the 1:1500 dilution of FTX, and the leak currents were similar. Figure 7B summarizes measurements of peak currents in many somatic patches in the absence and presence of purified FTX. It shows that FTX applied in the bath (for 3 min or more) before recording was no less effective in inhibiting Ca^{2+} channel currents than FTX included in the pipette solution. Figure 7C shows currents during voltage ramps from a patch at a dendritic bifurcation under control conditions and from 3 dendrites after prior exposure to purified FTX (1:600 dilution). The dendritic Ca^{2+} channel currents were reduced by FTX, as summarized in Figure 7D. (During the experiments depicted in Figures 7 and 8, relatively low resistance pipettes, <7 MΩ, were used so that currents were recorded in all control patches. Measurements were taken only from those patches with a resting potential more negative than −45 mV, which was measured at the end of each recording. The holding potentials varied between −90 mV and −75 mV.)

In Figure 7C, lower half, the approximate position of the patch pipette is indicated in the insets to the left of the traces. It appears that the size of the current not inhibited by FTX increased somewhat with distance from the soma, although we are aware that this deduction is based on few observations. That is, the currents recorded from a primary bifurcation not far from the soma (~30 μm) were completely inhibited by FTX (Figure 7C, top trace). A small current (−0.9 pA) could be recorded with FTX at a primary bifurcation separated from the soma by a relatively long proximal dendrite (~60 μm; Figure 7C, middle trace). At a third order bifurcation further away from the soma (~100 μm), the current remaining in the presence of FTX, while much smaller than the control, was larger than that at the more proximal sites (−1.6 pA; Figure 7C, lower trace). This suggests the presence of a larger number of channels at the peripheral than at the proximal dendrites. Another possibility is that a different type of channel is operant in the peripheral dendrite, although virtually all of the dendritic Ca^{2+} channels can be blocked by purified FTX, in the presence of physiological concentrations of divalent cations (Tank et al., 1988; Llinás et al., 1989).

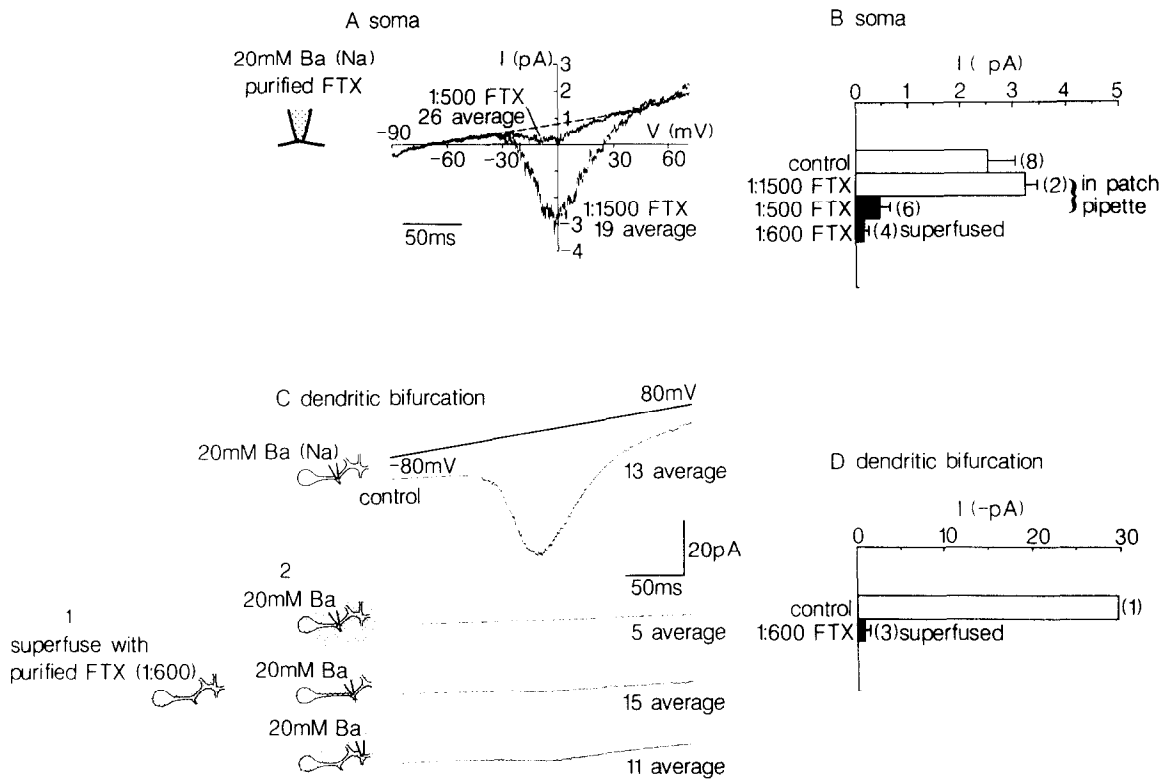The I–V relationships of 20 mM Ba^{2+} currents were similar in the absence and presence of FTX. Under

A soma

20mM Ba (Na)
purified FTX

I (pA) 3

1:500 FTX 2
26 average 1
-90
-60 -30 30 60
V (mV)

1:1500 FTX
19 average
-3
-4

50ms

B soma

I (pA)
0 1 2 3 4 5

control
1:1500 FTX (2)
1:500 FTX (6)
1:600 FTX (4)superfused

(8) in patch
pipette

C dendritic bifurcation

20mM Ba (Na)
-80mV
control

80mV

13 average

20pA
50ms

2
20mM Ba
5 average

1
superfuse with
purified FTX (1:600)

20mM Ba
15 average

20mM Ba
11 average

D dendritic bifurcation

I (-pA)
0 10 20 30

control
1:600 FTX (3)superfused
(1)

Figure 7. P-type Ca²⁺ Channels in the Somata and Dendrites of Purkinje Cells Are Blocked by Purified FTX

(A) Left: Partially purified FTX was added to a pipette solution containing 20 mM Ba²⁺ and Na⁺. Na⁺ channels were blocked by 1 μM TTX. Right: Superimposed average currents recorded in two somatic patches with a 1:500 or 1:1500 dilution of FTX. Currents were evoked by voltage ramps. For both recordings, R_p, ~7 MΩ. R_s, ~90 GΩ. Filter, 1.9 kHz.

(B) Peak 20 mM Ba²⁺ currents (corrected for leak currents) recorded in somatic patches without FTX, with different concentrations of FTX in the pipette, or without FTX in the pipette from somata bathed in FTX.

(C) 20 mM Ba²⁺ currents evoked by voltage ramps in dendritic patches. Top: Averaged current from a primary bifurcation in the absence of FTX. Lower three traces: Averaged currents at three bifurcations in the presence of purified FTX (1:600 dilution). 1: FTX was applied in the bath solution. 2: Recordings were then made with FTX-free pipette solutions. The approximate positions of the recording pipettes are indicated to the left of the current traces. R_p, 6-7 MΩ. R_s, 30-40 GΩ. Filter, 1.9 kHz.
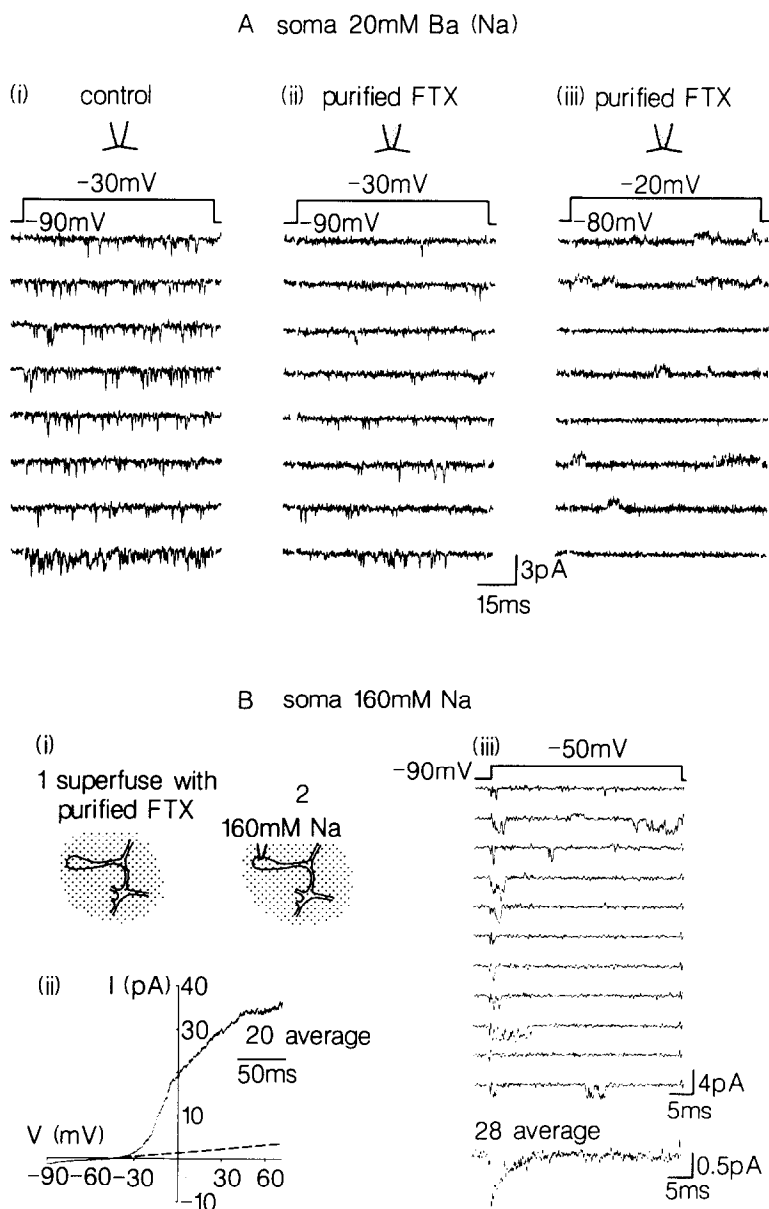
(D) Amplitudes of peak currents in (C), corrected for leak currents.

control conditions, the currents elicited by depolarizing ramps showed a threshold of activation of -36 ± 1.6 mV in 8 somatic patches and a single peak at -6 ± 2 mV. The currents in 2 dendritic patches activated at -33 mV and were maximal at -12 mV. (As expected from a screening effect of Ba²⁺ on surface potential, these parameters were more negative than those for 110 mM Ba²⁺ currents but more positive than those for 10 mM Ba²⁺ currents.) Small currents remaining in FTX activated at -31 ± 2 mV (pooling data from 7 somatic and 3 dendritic patches). A clear current peak could be measured in 3 somatic patches and 1 dendritic patch at -7 ± 2 mV.

As mentioned above, depolarizing voltage ramps were always immediately followed by hyperpolarizing ramps back to the holding potential (data not shown). When FTX completely inhibited the current during a depolarizing ramp, it also completely inhibited the current during a hyperpolarizing ramp. In other patches, currents remaining in the presence of FTX generated by depolarizing and hyperpolarizing ramps were of similar size and showed a similar I-V relation-

ship. To investigate further the mode of action of FTX, unitary Ca²⁺ channel currents carried by 20 mM Ba²⁺ during ~70 ms voltage jumps were recorded in the absence (10 somatic patches) or presence (1:600 or 1:500 dilution, 6 somatic and 2 dendritic patches) of FTX. Figure 8A shows examples of these in a somatic patch under control conditions and in 2 somatic patches with purified FTX in the pipette. FTX reduced the number of inward single-channel currents (Figure 8A, ii) or abolished them (iii). Inward currents remaining in the presence of FTX occurred throughout the jumps (Figure 8A, ii). In 4/4 somatic patches in which the Ca²⁺ channel currents were virtually abolished, unitary outward K⁺ currents remained in the presence of FTX (Figure 8A, iii). The results of both the voltage-ramp and voltage-jump experiments suggest that the effect of FTX was to reduce the probability of Ca²⁺ channel opening, without altering voltage dependence of activation and without increasing time-dependent inactivation.

The outward currents remaining in the presence of FTX (see above and Figure 8A, iii) suggested that FTX

A soma 20mM Ba (Na)

(i) control

ᴗ
-30mV
⌐-90mV⌐

(ii) purified FTX

ᴗ
-30mV
⌐-90mV⌐

(iii) purified FTX

ᴗ
-20mV
⌐-80mV⌐

_|3pA
15ms

Figure 8. P-type Ca^{2+} Channels, but Not K^+ or Na^+ Channels, in Adult Purkinje Cells Are Blocked by Purified FTX

(A) Single-channel recording in 3 somatic patches with a 20 mM Ba^{2+} pipette solution in which the other cation was Na^+. Na^+ channels were blocked by 1 μM TTX. (i) Unitary currents with control pipette solution. (ii) Reduced activity with purified FTX (1:500 dilution) in the pipette. Same patch as in Figure 7A. (iii) In this patch, FTX (1:500 dilution) abolished inward Ba^{2+} currents, but not outward K^+ currents. R_p, 7–9 MΩ. R_s, 60–100 GΩ. Filter, 1.9 kHz.

(B) FTX-resistant Na^+ and K^+ currents in a somatic patch. (i) 1: The bath was perfused with purified FTX (1:600 dilution). 2: Cell-attached recordings were then made from the soma with a Ca^{2+}-free Na^+ pipette solution. (ii) Average current recorded during depolarizing voltage ramps. There is a clear outward K^+ current, which is 31 pA, at +70 mV (corrected for the leak current indicated by the dashed line). (iii) Na^+ currents evoked by depolarizing voltage jumps. Shown are 8 consecutive current sweeps and the average of 28 sweeps (including empty ones). The Na^+ current is too small to be seen in (ii). R_p, 6 MΩ; R_s, 40 GΩ. Filter, 1.9 kHz (ii and iii).

B soma 160mM Na

(i)
1 superfuse with purified FTX
2
160mM Na

(ii) I (pA) 40
30
20 average
50ms
10
V (mV)
-90 -60 -30 | 30 60
-10

(iii) -50mV
-90mV⌐ ⌐

_|4pA
5ms
28 average
_|0.5pA
5ms

was selective for Ca^{2+} channels over K^+ channels. Additional experiments suggested that, at dilutions that reduce Ca^{2+} channel currents by ~85%, purified FTX has little effect on K^+ or Na^+ channels. In one set of experiments, the cell was bathed in a ~1:600 dilution of FTX and cell-attached recordings were made with a 160 mM Na^+ pipette solution (Figure 8B, i). This pipette solution was Ca^{2+} free so that voltage-dependent, but not Ca^{2+}-dependent, K^+ channels would be activated. Figure 8B, ii, illustrates the outward K^+ current generated in a somatic patch by a depolarizing voltage ramp after exposure to FTX. It was +31 pA at the end of the ramp (~+70 mV), which is similar to the average current of +39 pA recorded in the absence of FTX from 2 somatic patches. Figure 8B, iii, illustrates single Na^+ channel currents that were not inhibited by FTX (same patch as in Figure 8B, ii). In a second set of experi-

ments, currents were recorded with the bathing solution containing 2.4 mM Ca^{2+} in the cell-attached pipette. The average control outward current in 4 somatic patches was +131 ± 60 pA at ~+70 mV. After exposure to FTX, the current in 1 somatic patch was +29 pA. The difference may represent currents through Ca^{2+}-activated K^+ channels that are inoperative because the Ca^{2+} channels have been blocked by FTX.

Discussion

Purkinje Cells Lack T-type Ca^{2+} Channels

From the biophysical properties of the Ba^{2+} currents recorded, it is apparent that adult Purkinje cells lack T-type channels in both the soma and the dendrite, in agreement with the conclusion reached from intracel-

lular voltage recording in adult Purkinje cells (Llinás and Sugimori, 1980a, 1980b). In contrast, previous patch-clamp studies identified T-type channels (Bossu et al., 1989a, 1989b; Regan, 1989, 1991). However, these patch-clamp experiments were on immature rather than adult Purkinje cells. Furthermore, while many cultured Purkinje cells derived from newborn or embryonic rats exhibit T-type currents, only a fraction of cell bodies freshly dissociated from slightly older animals (1–3 week postnatal rats) demonstrate T-type channels. One proposal that can accommodate these observations is that T-type channels are present in immature Purkinje cells and that they disappear with development, as is the case in hippocampal pyramidal cells (Thompson and Wong, 1991). The observations in both Purkinje and hippocampal neurons fit in with the supposition that the role of T-type channels in young neurons is to generate autorhythmic behavior, which induces proper connectivity during development (Llinás, 1987).

Pharmacology of High Threshold Ca²⁺ Channels in Adult Cerebellar Purkinje Cells

The high threshold Ca²⁺ channels in the somata and dendrites of Purkinje cells are pharmacologically distinct from high threshold N- and L-type channels, since they were not inhibited by ω-CgTx and were not enhanced by BAY K 8644. They could, however, be inhibited by purified FTX. This unique pharmacology supports their definition as P-type channels, suggested on the basis of earlier experiments (Llinás et al., 1989).

The concentrations of FTX used were high compared with those tested in other systems (Sullivan and Lasater, 1992; Uchitel et al., 1992; see Bertolino and Llinás, 1992). These were necessary since currents were recorded with Ba²⁺ rather than Ca²⁺ (Lin et al., 1990), and in experiments in which FTX was included in the recording pipette, we believed that a rapid effect of a higher concentration of FTX would be more definitive than a gradual decline of the current induced by a lower concentration of FTX. Additional experiments are required to determine the mechanism of block by FTX. Our data suggest that it reduces the probability of opening without markedly altering time-dependent inactivation or the voltage dependence of activation. We did not test for use dependence of block by FTX and did not examine the effect of FTX on single-channel conductance, on steady-state inactivation, or on T-, N-, or L-type channels in other types of neurons.

FTX is a small (200–400 daltons), nonpeptide compound (Llinás et al., 1989; Cherksey et al., 1991) and is therefore distinct from the peptide ω-Aga-IVA (~ 5203 daltons), which can also be purified from the venom of Agenelopsis aperta (Mintz et al., 1992a). P-type channels can also be blocked by ω-Aga-IVA (Mintz et al., 1992b) and by the recently described peptide ω-conotoxin MVIIC (Hillyard et al., 1992). The effect of ω-AGA-IVA is voltage dependent; it is relieved by

persistent depolarization to positive potentials (>+70 mV; Mintz et al., 1992b). It is not known whether the effect of FTX is also relieved by prolonged depolarization.

We compared results from different membrane patches with and without drugs. It is therefore possible that our experiments may have overlooked some channels blocked by ω-CgTx or activated by BAY K 8644. However, if these types of channels were present (Ahlijanian et al., 1990) and not detected, they must contribute only a very minor portion of the Ca²⁺ channel current (Regan et al., 1991) or be located in regions from which recordings were not made. We find that the pharmacology of Ca²⁺ channels in adult Purkinje cells is not the same as that of high threshold Ca²⁺ channels in cultured cells (Bossu et al., 1989b). The difference may arise not only because cultured Purkinje cells were derived from embryonic or newborn rats (see above), but also because the development of Ca²⁺ channels in these cells is profoundly affected by culture conditions (Bossu et al., 1989a).

Comparison of P-type Channels with N- and L-type Channels

With 110 mM Ba²⁺ as the charge carrier, the I–V curves of P-type channels were similar to those of N-type channels, but were more negative than the I–V curves of L-type channels in the absence of DHP agonists. For example, P-type currents activate at ~−15 mV, whereas N-type channels activate at ~−20 mV and L-type channels activate at ~0 mV (Fox et al., 1987b; Plummer et al., 1989). As suggested previously (Regan et al., 1991), the I–V curves of the various types of Ca²⁺ channels are less distinctive in lower concentrations of Ba²⁺. For instance, with 10 mM Ba²⁺ as the charge carrier, P-type channels activate at ~−45 mV, which is near the threshold of activation of N- and L-type channels in a variety of cells (e.g., Carbone et al., 1990; Usowicz et al., 1990; Kasai and Neher, 1992).

Are P-type channels characterized by a unitary conductance different from that of N- or L-type channels? P-type channels in the somata and dendrites of adult Purkinje cells show openings to conductance levels of 9, 14, and 19 pS. These are similar to the range of conductances reported for N- and L-type channels (Bean, 1989). Therefore, P-type channels cannot be distinguished from N- or L-type channels on the basis of single-channel conductance alone.

Comparison of P-type Channels with Other High Threshold Channels That Are Not L or N Type

Ca²⁺ channels that pharmacologically resemble P-type channels are the cloned BI brain Ca²⁺ channel and Ca²⁺ channels expressed in Xenopus oocytes from rat brain mRNA (Leonard et al., 1987; Lin et al., 1990; Mori et al., 1991). We find that P-type channels in Purkinje cells resemble these putative P-type channels not only in their pharmacology, but also in their I–V curves. Currents carried by 40–60 mM Ba²⁺ through the cloned BI channel and through the channel expressed from

brain mRNA activate between −30 and −20 mV and are maximal at ∼+20 mV. In comparison, 110 mM Ba²⁺ currents in adult Purkinje cells activate at ∼−15 mV and peak at ∼+10 mV, whereas 20 mM Ba²⁺ currents in adult Purkinje cells activate at −35 mV and peak at ∼−10 mV. Isolated P-type channels in lipid bilayers activate at more negative potentials for undetermined reasons (Llinás et al., 1989).

The single-channel conductances (9, 14, and 19 pS) of P-type channels in Purkinje cells are similar to those of the putative P-type channels and of P-type channels in lipid bilayers. The BI channel opens to a conductance level of 16 pS and to a smaller conductance, for which an estimate was not given (110 mM Ba²⁺; Mori et al., 1991). Ca²⁺ channels expressed in Xenopus oocytes from total brain mRNA open to conductances of 13 and 20 pS (70 mM Ba²⁺; Lin and Llinás, 1990, Soc. Neurosci., abstract). The conductances of P-type channels isolated from the cerebellum or squid optic lobe and inserted into lipid bilayers are 10–12 pS or 18–20 pS, respectively (80 mM Ba²⁺; Llinás et al., 1989).

Do these channels differ in their rates of time-dependent inactivation? Our experiments and those of Regan (1991) indicate that P-type channels exhibit little time-dependent inactivation. Similarly, Ca²⁺ channels expressed from total brain mRNA inactivate slowly: during a ∼300 ms jump to potentials between 0 and +20 mV, the macroscopic current decays by ∼20% (40–60 mM Ba²⁺; Leonard et al., 1987; Lin et al., 1990). In contrast, it is suggested that inactivation of BI channels is more rapid: the macroscopic current decays by ∼55% after 300 ms (40 mM Ba²⁺; Mori et al., 1991). However, it is unclear whether the rate of inactivation is affected by the α_2 and β subunits of the skeletal muscle DHP receptor, with which the BI channel was coexpressed. In fact, the pharmacological profiles, I–V curves, and single-channel conductances of the cloned BI channel and the Ca²⁺ channels expressed from brain mRNA imply that these channels may well belong to the P type.

High threshold Ca²⁺ channel currents resistant to blockers of N- and L- type channels have been observed in a variety of peripheral and central neurons in whole-cell voltage clamp (Kaneko et al., 1989; Mogul and Fox, 1991; Regan et al., 1991; Artalejo et al., 1992). Single-channel recording in one of these studies (Mogul and Fox, 1991) revealed only L- and N-type channels, identified by their unitary conductance. In other words, a novel conductance was not observed, and Mogul and Fox (1991) concluded that there may be a type of Ca²⁺ channel distinct from N- and L-type channels according to its pharmacology but not its elementary conductance. Our results support this conclusion. Furthermore, it is possible that any P-type channels present may have been blocked by BAY K 8644 that was present throughout the single-channel experiments of Mogul and Fox (1991), as suggested by our preliminary data and those of Mori et al. (1991). Moreover, reported unitary conductances for high threshold channels not classified as N- or L-type are

14 pS (Artalejo et al., 1992) and 9 and 14 pS (O'Dell and Alger, 1991). These values are the same as our measurements for P-type channels. It will be interesting to see whether these non-N-type or non-L-type channels are blocked by FTX, ω-Aga-IVA, or ω-conotoxin MVIIC.

There are reports of low threshold currents, in freshly dissociated Purkinje cells and in other types of neurons, with a pharmacology distinct from that of T-type channels (Akaike et al., 1989; Kaneda and Akaike, 1989; Takahashi and Akaike, 1990; Kaneda et al., 1990; Richard et al., 1991). It is intriguing that these channels, like P-type channels in Purkinje cells and the BI channel (Mori et al., 1991), are blocked by BAY K 8644 and other DHPs, albeit at concentrations higher than those selective for L-type channels. In most cases, recordings were made with Ca²⁺ as the charge carrier. It will be interesting to examine the properties of Ba²⁺ currents through these channels and to determine their elementary conductance and sensitivity to ω-CgTx, FTX, ω-Aga-IVA, and ω-conotoxin MVIIC.

Differential Distribution of P-type Channels in Somata and Dendrites

Our present finding of P-type Ca²⁺ channels in the soma, as well as in the dendrite, is in apparent contrast with the conclusion from intracellular recording and Ca²⁺ imaging experiments that Ca²⁺ channels in adult Purkinje cells are preferentially located in the dendrites (Llinás and Sugimori, 1980a, 1980b; Ross and Werman, 1987; Tank et al., 1988; Hockberger et al., 1989; Sugimori and Llinás, 1990). However, a low density of somatic Ca²⁺ channels (Hillman et al., 1991) would not generate sufficient voltage to be observable using conventional voltage recording techniques given the input impedance of the Purkinje cell and the large somatic K⁺ conductance (Llinás and Sugimori, 1980a, 1980b). Indeed, in somatic patches, we find outward K⁺ currents of +20 ± 11 pA at −15 mV (n = 4; evoked by depolarizing voltage ramps), which easily mask the peak Ca²⁺ current of −0.5 to −2.4 pA (recorded with 2.4 mM Ca²⁺, after outward K⁺ currents had been abolished; data not shown).

To understand the function of multiple types of Ca²⁺ channels, it is necessary to know their spatial distribution. So far, our preliminary experiments have not revealed any major differences between the pharmacology, I–V curves, and single-channel conductances of Ca²⁺ channels located in the soma and dendrite. In Figure 2, there is a subtle difference between the inward 110 mM Ba²⁺ currents recorded in the dendrite and the soma: the I–V relationship, between the activation and peak potentials, was steeper in the dendrite than in the soma. However, a statistical comparison of many somatic and dendritic patches is required to demonstrate quantitatively differences in channel density or the relative occurrence of the different conductances between these two membrane areas. Such analysis will also be needed to determine whether the somatic and dendritic channels have different kinet-

ics. The answers to these questions will not be obtained easily, however, given the technical difficulties associated with patch-clamp recording from dendrites and the tendency of the channels to cluster.

Experimental Procedures

Slice Preparation
Sagittal cerebellar slices (~150 µm thick) were prepared from adult guinea pigs, as previously described (Llinás and Sugimori, 1980a; Edwards et al., 1989). Briefly, female guinea pigs (Hartley; 150–350 g) were anesthetized with an intraperitoneal injection of sodium pentobarbital (~65 mg/kg) and decapitated. The cerebellum was removed into cold (6°C) Krebs-Henseleit solution composed of 124 mM NaCl, 5 mM KCl, 1.3 mM MgSO₄, 2.4 mM CaCl₂, 1.2 mM KH₂PO₄, 26 mM NaHCO₃, 10 mM D-glucose (pH 7.4 when bubbled with 95% O₂, 5% CO₂). Slices were cut with an Oxford G501 vibratome and stored at room temperature for at least 1 hr and up to 8 hr before recording.

Recording
Slices were secured on the glass bottom of a recording chamber with a fine net (Edwards et al., 1989) and viewed on an upright microscope (aus Jena) with a ~25× water immersion objective (total magnification ~500×; Leitz). They were superfused with a solution containing 133 mM NaCl, 2.5 mM KCl, 1.3 mM MgCl₂, 2.4 mM CaCl₂, 10 mM D-glucose, and 20 mM HEPES (pH 7.4 with NaOH), supplemented with 0.5 µM or 1 µM tetrodotoxin (TTX) and bubbled with O₂. The cleaning pipette (10–15 µm opening; Edwards et al., 1989) was filled with this HEPES solution. The bath was maintained at 22°C ± 1°C with a Peltier plate.

Cell-attached patch recordings (Hamill et al., 1981) were made with a List EPC7 amplifier. Patch pipettes (hard borosilicate glass; World Precision Instruments) were coated with Sylgard resin (184, Dow Corning), fire-polished, and filled with one of four solutions. These were a 110 mM Ba²⁺ solution (110 mM BaCl₂, 10 mM HEPES, 0 or 0.1 mM EGTA [pH 7.4 with TEA–OH]); a 10 mM Ba²⁺ solution (10 mM BaCl₂, 134 mM TEA-Cl, 10 mM HEPES, 0.1 mM EGTA, 10 mM CsCl [pH 7.4 with TEA–OH]); a 20 mM Ba²⁺ solution (20 mM BaCl₂, 135 mM NaCl, 10 mM HEPES, 0.1 mM EGTA [pH 7.4 with NaOH]) and a 160 mM Na⁺ solution (160 mM NaCl, 10 mM HEPES, 0.1 mM EGTA, 3 mM MgCl₂ [pH 7.4 with NaOH]). All of the Ba²⁺ solutions were supplemented with 0.5 or 1 µM TTX. The pipette and bath solutions were passed through a 0.22 µm Millipore filter. Measurements of the resistance of the pipette before (R_p) and after (R_s) formation of the pipette-membrane seal are given in the figure legends, when available (Hamill et al., 1981).

The potentials given in the text are the difference between the applied patch potential and the resting potential. The resting potential was either measured at the end of the recording, by breaking through the membrane into the whole-cell configuration, or taken as the average measured in other cells in the same set of slices. It was measured immediately after entering the whole-cell configuration, i.e., before the pipette solution had time to diffuse into the cell and alter the membrane potential. For clarity, values plotted in the figures have been rounded down to the nearest 5 mV. The average resting potential was −55 ± 1 mV (n = 53) in the soma and −50 ± 3 mV in the dendrite (n = 7). The stability of voltage-jump recording was assessed by choosing a voltage, jumping to it 5–10 times, once every few minutes of recording, and comparing the evoked channel activity or the leak currents. In voltage-ramp experiments, a decreasing resting potential was apparent as a leftward shift of the I–V curve. However, it is not certain that the measured resting potential was the same as that at the start of the recording or that it remained constant during the recording. Therefore, the quoted potentials may be in error by 5 to 10 mV, i.e., by no more than when the resting potential is zeroed with a high K⁺ solution (Winegar and Lansman, 1990). Given this limited accuracy, values were not corrected for junction potentials between the bath solution and the various pipette solutions, which varied between

−2 mV and +2 mV. All voltage ramps were applied from a holding potential set 30 mV negative to the resting potential. Voltage jumps were applied either from this hyperpolarized holding potential or from the resting potential.

Analysis
The pClamp computer software (v. 5.5.1, Axon Instruments) and the Labmaster A-D converter were used to generate command potentials and for analysis. Data are given as mean ± SEM. Recordings were stored on VHS video tape (with a Neurocorder, Neurodata Instruments) and later amplified, low pass-filtered at 4 kHz (70 ms jumps), 0.5 kHz (1100 ms jumps), or 2 kHz (ramps) (−3 dB, 8 pole Bessel), and acquired into a computer at a sample rate of 25 kHz (70 ms jumps), 1.66 kHz (1100 ms jumps), or 4.1 kHz (ramps). Currents evoked by 70 ms voltage jumps were filtered during analysis with a digital Gaussian filter (1.5–3 kHz). The effective cutoff frequencies were calculated from the filter settings of the amplifiers, the Bessel filter and the Gaussian filter (Colquhoun and Sigworth, 1983). They are given in the figure legends and were used to calculate the minimum resolvable durations (below).

Capacitive current transients were partially nulled with the amplifier during recording. Leak currents and the remaining capacity transients were removed during analysis from openings activated by voltage jumps by subtracting the average of sweeps with no openings, with or without appropriate scaling. The correction was not usually applied to currents during voltage ramps, which are consequently noisier.

Single-channel currents were analyzed manually with the 50% threshold crossing method. The baseline and open levels were continuously adjusted to keep the threshold at the 50% level. The resultant list of measurements was revised by imposing a minimum resolvable duration for openings and closings (Colquhoun and Sigworth, 1983). This was set at a value (320–480 µs) equal to 2 times the rise time of the effective filter before forming amplitude histograms, or at 1.6 times the rise time of the filter for open time histograms (240 µs). The amplitude histograms were fitted by Gaussian curves (data not shown); the open time histograms were fitted by two exponential components with the Levenberg–Marquardt nonlinear least squares method. The unitary current amplitude was determined from the Gaussian curves, or when the number of openings was low, it was calculated as the arithmetic mean of measurements made with cursors.

Drugs
The 1,4-DHP (±) BAY K 8644 (Research Biochemical Inc.) was prepared on the day of the experiment as 10 or 30 mM stock solutions in tissue culture quality dimethylsulfoxide or, occasionally, in 100% ethanol. Control experiments showed that dimethylsulfoxide or ethanol at 0.01% or 0.03% (the final concentrations in pipettes containing BAY K 8644) did not inhibit the Ca²⁺ channels. Because of the light sensitivity and potential nonspecific binding of DHPs to plastic, BAY K 8644 was prepared and applied in near darkness, with glass apparatus. Synthetic ω-CgTx (Peninsula Laboratories) was prepared as 0.5 or 1 mM solutions in distilled water and stored in aliquots at −20°C. Dilutions of purified FTX are expressed relative to the crude venom. For example, if the active fraction was collected in a volume of 1 ml and the starting volume of crude venom was 200 µl, this represents a dilution of 1:5, assuming that all of the toxin present in the venom was recovered. If this was further diluted 100 times into the pipette or bathing solutions before the experiment, the total dilution was 1:500.

by the payment of page charges. This article must therefore be hereby marked "advertisement" in accordance with 18 USC Section 1734 solely to indicate this fact.

References

Abe, T., Koyano, K., Saisu, H., Nishiuchi, Y., and Sakakibara, S. (1986). Binding of ω-conotoxin to receptor sites associated with the voltage-sensitive calcium channel. Neurosci. Lett. 71, 203–208.

Ahlijanian, M. K., Westenbroek, R. E., and Catterall, W. A. (1990). Subunit structure and localization of dihydropyridine-sensitive calcium channels in mammalian brain, spinal cord, and retina. Neuron 4, 819–832.

Akaike, N., Kostyuk, P. G., and Osipchuk, Y. V. (1989). Dihydropyridine-sensitive low-threshold calcium channels in isolated rat hypothalamic neurones. J. Physiol. 412, 181–195.

Aosaki, T., and Kasai, H. (1989). Characterization of two kinds of high-voltage-activated Ca-channel currents in chick sensory neurones. Differential sensitivity to dihydropyridines and ω-conotoxin GVIA. Pflügers Arch. 414, 150–156.

Artalejo, C. R., Perlman, R. L., and Fox, A. P. (1992). ω-Conotoxin blocks a Ca²⁺ current in bovine chromaffin cells that is not of the "classic" N type. Neuron 8, 85–95.

Bean, B. P. (1989). Classes of calcium channels in vertebrate cells. Annu. Rev. Physiol. 51, 367–384.

Bechem, M., Hebisch, S., and Schramm, M. (1988). Ca²⁺ agonists: new, sensitive probes for Ca²⁺ channels. Trends Pharmacol. Sci. 9, 257–261.

Bertolino, M., and Llinás, R. R. (1992). The central role of voltage-activated and receptor-operated calcium channels in neuronal cells. Annu. Rev. Pharmacol. Toxicol. 32, 399–421.

Boll, W., and Lux, H. D. (1985). Action of organic antagonists on neuronal calcium currents. Neurosci. Lett. 56, 335–339.

Bossu, J.-L., Dupont, J.-L., and Feltz, A. (1989a). Calcium currents in rat cerebellar Purkinje cells maintained in culture. Neuroscience 30, 605–617.

Bossu, J.-L., Fagni, L., and Feltz, A., (1989b). Voltage-activated calcium channels in rat Purkinje cells maintained in culture. Pflügers Arch. 414, 92–94.

Brown, A. M., Kunze, D. L., and Yatani, A. (1984). The agonist effect of dihydropyridines on Ca channels. Nature 311, 570–572.

Carbone, E., and Lux, H. D. (1984a). A low voltage-activated, fully inactivating Ca channel in vertebrate sensory neurones. Nature 310, 501–502.

Carbone, E., and Lux, H. D. (1984b). A low voltage-activated calcium conductance in embryonic chick sensory neurons. Biophys. J. 46, 413–418.

Carbone, E., Sher, E., and Clementi, F. (1990). Ca currents in human neuroblastoma IMR32 cells: kinetics, permeability and pharmacology. Pflügers Arch. 416, 170–179.

Cherksey, B. D., Sugimori, M., and Llinás, R. R. (1991). Properties of calcium channels isolated with spider toxin, FTX. Ann. NY Acad. Sci. 635, 80–89.

Colquhoun, D., and Sigworth, F. J. (1983). Fitting and statistical analysis of single-channel records. In Single-Channel Recording, B. Sakmann and E. Neher, eds. (New York: Plenum Publishing Corp.), pp. 191–263.

Edwards, F. A., Konnerth, A., Sakmann, B., and Takahashi, T. (1989). A thin slice preparation for patch clamp recordings from neurones of the mammalian central nervous system. Pflügers Arch. 414, 600–612.

Fedulova, S. A., Kostyuk, P. G., and Veselovsky, N. S. (1985). Two types of calcium channels in the somatic membrane of newborn rat dorsal root ganglion neurones. J. Physiol. 359, 431–446.

Fox, A., Nowycky, M. C., and Tsien, R. W. (1987a). Kinetic and pharmacological properties distinguishing three types of cal-

cium currents in chick sensory neurones. J. Physiol. 394, 149–172.

Fox, A., Nowycky, M. C., and Tsien, R. W. (1987b). Single-channel recordings of three types of calcium channels in chick sensory neurones. J. Physiol. 394, 173–200.

Hamill, O. P., Marty, A., Neher, E., Sakmann, B., and Sigworth, F. J. (1981). Improved patch-clamp techniques for high-resolution current recording from cells and cell-free membrane patches. Pflügers Arch. 391, 85–100.

Hess, P. (1990). Calcium channels in vertebrate cells. Annu. Rev. Neurosci. 13, 337–356.

Hess, P., Lansman, J. B., and Tsien, R. W. (1984). Different modes of Ca channel gating behaviour favoured by dihydropyridine Ca agonists and antagonists. Nature 311, 538–544.

Hillman, D., Chen, S., Aung, T. T., Cherksey, B., Sugimori, M., and Llinás, R. R. (1991). Localization of P-type calcium channels in the central nervous system. Proc. Natl. Acad. Sci. USA 88, 7076–7080.

Hillyard, D. R., Monje, V. D., Mintz, I. M., Bean, B. P., Nadasdi, L., Ramachandran, J., Miljanich, G., Azimi-Zoonooz, A., McIntosh, J. M., Cruz, L. J., Imperial, J. S., and Olivera, B. M. (1992). A new conus peptide ligand for mammalian presynaptic Ca²⁺ channels. Neuron 9, 69–77.

Hirano, T., and Hagiwara, S. (1989). Kinetics and distribution of voltage-gated Ca, Na and K channels on the somata of rat cerebellar Purkinje cells. Pflügers Arch. 413, 463–469.

Hockberger, P. F., Tseng, H.-Y., and Connor, J. A. (1989). Fura-2 measurements of cultured rat Purkinje neurons show dendritic localization of Ca²⁺ influx. J. Neurosci. 9, 2272–2284.

Jones, S. W., and Jacobs, L. S. (1990). Dihydropyridine actions on calcium currents of frog sympathetic neurons. J. Neurosci. 10, 2261–2267.

Kaneda, M., and Akaike, N. (1989). The low-threshold Ca current in isolated amygdaloid neurons in the rat. Brain Res. 497, 187–190.

Kaneda, M., Wakamori, M., Ito, C., and Akaike, N. (1990). Low-threshold calcium current in isolated Purkinje cell bodies of rat cerebellum. J. Neurophysiol. 63, 1046–1051.

Kaneko, A., Pinto, L. H., and Tachibana, M. (1989). Transient calcium current of retinal bipolar cells of the mouse. J. Physiol. 410, 613–629.

Kasai, H., and Neher, E. (1992). Dihydropyridine-sensitive and ω-conotoxin-sensitive calcium channels in a mammalian neuroblastoma-glioma cell line. J. Physiol. 448, 161–188.

Knaus, H.-G., Striessnig, J., Koza, A., and Glossmann, H. (1987). Neurotoxin aminoglycoside antibiotics are potent inhibitors of [¹²⁵I]-omega-conotoxin GVIA binding to guinea-pig cerebral cortex membranes. Naunyn Schmiedebergs Arch. Pharmacol. 336, 583–586.

Leonard, J. P., Nargeot, J., Snutch, T. P., Davidson, N., and Lester, H. A. (1987). Ca channels induced in Xenopus oocytes by rat brain mRNA. J. Neurosci. 7, 875–881.

Lin, J.-W., Rudy, B., and Llinás, R. (1990). Funnel-web spider venom and a toxin fraction block calcium current expressed from rat brain mRNA in Xenopus oocytes. Proc. Natl. Acad. Sci. USA 87, 4538–4542.

Llinás, R. (1987). 'Mindness' as a functional state of the brain. In Mindwaves. Thoughts on Intelligence, Identity and Consciousness, C. Blakemore and S. Greenfield, eds. (Oxford: Basil Blackwell).

Llinás, R. R. (1988). The intrinsic electrophysiological properties of mammalian neurons: insights into central nervous system function. Science 242, 1654–1664.

Llinás, R., and Sugimori, M. (1980a). Electrophysiological properties of in vitro Purkinje cell somata in mammalian cerebellar slices. J. Physiol. 305, 171–195.

Llinás, R., and Sugimori, M. (1980b). Electrophysiological properties of in vitro Purkinje cell dendrites in mammalian cerebellar slices. J. Physiol. 305, 197–213.

Llinás, R., and Yarom, Y. (1981). Properties and distribution of ionic conductances generating electroresponsiveness of mammalian inferior olivary neurones in vitro. J. Physiol. 315, 569–584.

Llinás, R., Sugimori, M., Lin, J.-W., and Cherksey, B. (1989). Blocking and isolation of a calcium channel from neurons in mammals and cephalopods utilizing a toxin fraction (FTX) from funnel-web spider poison. Proc. Natl. Acad. Sci. USA 86, 1689–1693.

Llinás, R., Sugimori, M., Hillman, D. E., and Cherksey, B. (1992). Distribution and functional significance of the P-type, voltage-dependent Ca²⁺ channels in the mammalian central nervous system. Trends Neurosci. 15, 351–355.

Marqueze, M., Martin-Moutot, N., Levêque, C., and Couraud, F. (1988). Characterization of the ω-conotoxin-binding molecule in rat brain synaptosomes and cultured neurons. Mol. Pharmacol. 34, 87–90.

McCleskey, E. W., Fox, A. P., Feldman, D. H., Cruz, L. J., Olivera, B. M., Tsien, R. W., and Yoshikami, D. (1987). ω-Conotoxin: direct and persistent blockade of specific types of calcium channels in neurons but not muscle. Proc. Natl. Acad. Sci. USA 84, 4327–4331.

Mintz, I. M., Venema, V. J., Swiderek, K. M., Lee, T. D., Bean, B. P., and Adams, M. E. (1992a). P-type calcium channels blocked by the spider toxin ω-Aga-IVA. Nature 355, 827–829.

Mintz, I. M., Adams, M. E., and Bean, B. P. (1992b). P-type calcium channels in rat central and peripheral neurons. Neuron 9, 85–95.

Mogul, D. J., and Fox, A. P. (1991). Evidence for multiple types of Ca²⁺ channels in acutely isolated hippocampal CA3 neurones of the guinea-pig. J. Physiol. 433, 259–281.

Mori, Y., Friedrich, T., Kim, M.-S., Mikami, A., Nakai, J., Ruth, P., Bosse, E., Hofmann, F., Flockerzi, V., Furuichi, T., Mikoshiba, K., Imoto, K., Tanabe, T., and Numa, S. (1991). Primary structure and functional expression from complementary DNA of a brain calcium channel. Nature 350, 398–402.

Nowycky, M. C., Fox, A. P., and Tsien, R. W. (1985a). Three types of neuronal calcium channel with different calcium agonist sensitivity. Nature 316, 440–443.

Nowycky, M. C., Fox, A. P., and Tsien, R. W. (1985b). Long-opening mode of gating of neuronal calcium channels and its promotion by the dihydropyridine calcium agonist Bay K 8644. Proc. Natl. Acad. Sci. USA 82, 2178–2182.

O'Dell, T. J., and Alger, B. E. (1991). Single calcium channels in rat and guinea-pig hippocampal neurones. J. Physiol. 436, 739–767.

Plummer, M. R., Logothetis, D. E., and Hess, P. (1989). Elementary properties and pharmacological sensitivities of calcium channels in mammalian peripheral neurons. Neuron 2, 1453–1463.

Porzig, H. (1990). Pharmacological modulation of voltage-dependent calcium channels in intact cells. Rev. Physiol. Biochem. Pharmacol. 114, 210–262.

Regan, L. J. (1989). Calcium channels in freshly dissociated rat cerebellar Purkinje cells. Ann. NY Acad. Sci. 560, 121–123.

Regan, L. J. (1991). Voltage-dependent calcium currents in Purkinje cells from rat cerebellar vermis. J. Neurosci. 11, 2259–2269.

Regan, L. J., Sah, D. W. Y., and Bean, B. P. (1991). Ca²⁺ channels in rat central and peripheral neurons: high-threshold current resistant to dihydropyridine blockers and ω-conotoxin. Neuron 6, 269–280.

Richard, S., Diochot, S., Nargoet, J., Baldy-Moulinier, M., and Valmier, J. (1991). Inhibition of T-type calcium currents by dihydropyridines in mouse embryonic dorsal root ganglion neurons. Neurosci. Lett. 132, 229–234.

Ross, W. N., and Werman, R. (1987). Mapping calcium transients in the dendrites of Purkinje cells from the guinea-pig cerebellum in vitro. J. Physiol. 389, 319–336.

Sugimori, M., and Llinás, R. R. (1990). Real-time imaging of calcium influx in mammalian cerebellar Purkinje cells in vitro. Proc. Natl. Acad. Sci. USA 87, 5084–5088.

Sullivan, J. M., and Lasater, E. M. (1992). Sustained and transient calcium currents in horizontal cells of the white bass retina. J. Gen. Physiol. 99, 85–107.

Takahashi, K., and Akaike, N. (1990). Nicergoline inhibits T-type Ca²⁺ channels in rat isolated hippocampal CA1 pyramidal neurones. Br. J. Pharmacol. 100, 705–710.

Tank, D. W., Sugimori, M., Connor, J. A., and Llinás, R. R. (1988). Spatially resolved calcium dynamics of mammalian Purkinje cells in cerebellar slice. Science 242, 773–777.

Thompson, S. M., and Wong, R. K. S. (1991). Development of calcium current subtypes in isolated rat hippocampal pyramidal cells. J. Physiol. 439, 671–689.

Triggle, D. J., and Ramp, D. (1989). 1,4-Dihydropyridine activators and antagonists: structural and functional distinctions. Trends Pharmacol. Sci. 10, 507–511.

Tsien, R. W., and Tsien, R. Y. (1990). Calcium channels, stores and oscillations. Annu. Rev. Cell Biol. 6, 715–760.

Tsien, R. W., Ellinor, P. T., and Horne, W. A. (1991). Molecular diversity of voltage-dependent Ca²⁺ channels. Trends Pharmacol. Sci. 12, 349–354.

Uchitel, O. D., Protti, D. A., Sanchez, V., Cherksey, B. D., Sugimori, M., and Llinás, R. (1992). P-type voltage-dependent calcium channel mediates presynaptic calcium influx and transmitter release in mammalian synapses. Proc. Natl. Acad. Sci. USA 89, 3300–3333.

Usowicz, M. M., Porzig, H., Becker, C., and Reuter, H. (1990). Differential expression by nerve growth factor of two types of Ca²⁺ channels in rat phaeochromocytoma cell lines. J. Physiol. 426, 95–116.

Wagner, J. A., Snowman, A. M., Biswas, A., Olivera, B. M., and Snyder, S. H. (1988). ω-Conotoxin GVIA binding to a high-affinity receptor in brain: characterization, calcium sensitivity, and solubilization. J. Neurosci. 8, 3354–3359.

Winegar, B. D., and Lansman, J. B. (1990). Voltage-dependent block by zinc of single calcium channels in mouse myotubes. J. Physiol. 425, 563–578.

Note Added in Proof

M. M. Usowicz's present address is the Department of Pharmacology, University of Bristol, Bristol, England.

Reprint requests should be addressed to R. Llinás.